npj | clean water

Article

Published in partnership with King Fahd University of Petroleum & Minerals

https://doi.org/10.1038/s41545-025-00519-6

Cyclodextrin polymer networks synthesis via amine-functionalized tripodal crosslinker for ultra-rapid removal of PFAS from water

Monu Verma[1], Youngmin Hong[1], Krishna Pal Singh[2], Vinod Kumar[3,4], Shu-Yuan Pan[5], Cong Li[6], Gyandshwar Kumar Rao[7], Manisha Nanda[8], Sanjay Kumar Arora[9] & Hyunook Kim[1]

Herein, we developed a β-cyclodextrin (β-CD)-based polymer crosslinked with tripodal amine to demonstrate the synergetic effects of the superior adsorption of both short- and long-chain per- and polyfluoroalkyl substances (PFASs). Kinetics studies showed rapid adsorption (~100% for nine PFASs at 1 μg L^{-1}, except PFBA, and >86% at 200 μg L^{-1} individually) within 2 min. Isotherm results showed exceptional adsorption affinity and capacity, with $K_L = 0.310 \pm 0.180$ L mg^{-1}, $q_m = 246.20 \pm 14.80$ mg g^{-1} for PFBS, and $K_L = 0.980 \pm 0.260$ L mg^{-1}, $q_m = 587.10 \pm 54.50$ mg g^{-1} for PFOS, significantly outperforming traditional activated carbons and resins. Adsorbent performed effectively in PFASs-spiked industrial wastewater with 55–100% removal efficiencies, regardless of the presence of co-contaminants. The adsorption mechanism confirmed the combined role of hydrophobic inclusion within β-CD cavities and electrostatic interactions with amine groups. Overall, this work demonstrates an advanced molecular design strategy for the PFAS-contaminated water and wastewater treatment.

Per- and polyfluoroalkyl substances (PFASs) are a class of highly stable fluorinated compounds that are widely used in various commercial and industrial applications, including waterproofing textiles, semiconductor manufacturing, firefighting activities, cosmetics, food packaging, and non-stick cookware coatings[1,2]. Their widespread use is attributed to their unique physicochemical properties such as high surface activity, amphiphilic characteristics (both hydrophilic and hydrophobic), and exceptional chemical and thermal stability[2–4]. However, their pervasive presence has resulted in global contamination of water resources. In addition, their bioaccumulation, toxicity, and persistence in the environment, even at low chronic exposure levels, have raised significant concerns within the scientific community, driving efforts to prevent and mitigate PFAS contamination[1,5,6]. Among the different PFASs, long-chain perfluorocarboxylic acids (PFCAs) and perfluorosulfonic acids (PFSAs) represent a broadly detected class, with regulatory efforts primarily focused on long-chain PFASs such as eight-carbon perfluorooctanoic acid (PFOA) and perfluorooctanesulfonic acid (PFOS). These long-chain PFASs have higher toxicity and are resistant to degradation. Therefore, in response to regulatory restrictions on long-chain PFASs, short-chain derivatives, such as four-carbon perfluorobutanoic acid (PFBA) and perfluorobutanesulfonic acid (PFBS), have been introduced as alternatives for many processes. However, emerging studies have revealed that these short-chain PFASs also pose toxicity concerns, exhibit greater environmental mobility, and demonstrate increased resistance to degradation and removal compared to their long-chain counterparts[7,8]. Therefore, developing effective treatment and remediation strategies for PFASs, particularly short-chain variants, is an urgent scientific and environmental priority.

Adsorption is one of the most promising approaches for treating PFAS-contaminated water[4,9]. Among the different types of conventional adsorbents, activated carbons (ACs) are most commonly employed in full-

[1]Water-Energy Nexus Laboratory, Department of Environmental Engineering, University of Seoul, Seoul, Republic of Korea. [2]Department of Chemistry, DAV (PG) College Muzaffarnagar, Muzaffarnagar, India. [3]Department of Food Science and Technology, Graphic Era (Deemed to Be University), Dehradun, India. [4]Peoples' Friendship University of Russia (RUDN University), Moscow, Russian Federation. [5]Department of Bioenvironmental Systems Engineering, National Taiwan University, Taipei, Taiwan. [6]School of Environment and Architecture, University of Shanghai for Science and Technology, Shanghai, China. [7]Department of Chemistry, Kisan College Sohsarai, Nalanda, Ashanagar, Bihar Sharif, India. [8]Department of Microbiology, Graphic Era (Deemed to Be University), Dehradun, India. [9]Department of Chemistry, SD College Muzaffarnagar, Muzaffarnagar, India. e-mail: h_kim@uos.ac.kr

scale adsorption processes[10,11]. However, they suffer from moderate to low affinity for PFASs, particularly for short-chain PFASs, and demonstrate slow diffusion-limited adsorption kinetics[12–14]. These shortcomings have been minimized using anion-exchange (AE) resins, but suffer from fouling issues caused by dissolved natural organic matters (NOM) and inorganic constituents, commonly found in water systems, making them a costly and inefficient solution[12,15]. These challenges highlight the urgent need to develop other advanced adsorbents, such as chitosan beads[16], cyclodextrin polymers[1,17–19], metal organic frameworks (MOF)[20,21], and covalent organic frameworks (COF)[3,22], to effectively remove both short-chain and long-chain PFASs at trace concentrations (μg L^{-1}). However, it is still needed to develop new adsorbents for the rapid removal of PFASs at the same concentration.

Insoluble polymer networks based on β-cyclodextrin (β-CD) have emerged as highly effective adsorbents for PFASs removal[1,4,17–19]. β-CDs are non-toxic, commercially available, macrocyclic oligosaccharides composed of seven glucose subunits and have been extensively studied for the removal of organic micropollutants through adsorption and membrane separation processes[23]. The unique structure of β-CD features a hydrophobic inner cavity to form host-guest inclusion complexes with many organic micropollutants, including PFASs of appropriate sizes and shapes[4,24–27]. β-CD exhibits strong association constants of 5.0×10^5 and 7.0×10^5 M^{-1} for the 1:1 host-guest complexes, i.e., β-CD-PFOA and β-CD-PFOS, respectively[28]. Interestingly, these β-CD-based cross-linked adsorbents demonstrate higher adsorption affinity, targeted selectivity towards PFASs, and rapid adsorption kinetics with rate constants 15–200 times higher than those of non-cross-linked CDs and ACs. These properties are highly dependent on the crosslinking segments and types of crosslinker. They adjust the adsorption capacity, kinetics, and selectivity of the adsorbents towards different PFASs. For example, a polymer network with tetrafluoroterephthalonitrile (TFN) linkers exhibited an excellent removal rate for cationic and neutral organic micropollutants compared to ACs[29]. However, the presence of anionic phenolate groups, which were introduced during the polymerization process, resulted in variable affinity, predominantly favoring neutral and cationic micropollutants, while exhibiting poor adsorption of anionic species, including PFOA[19]. However, the post-polymerization reduction of the nitrile groups of TFN into amino groups, which remain in a cationic form at neutral and acidic pHs, reversed its selectivity to yield a higher affinity for the effective removal of anionic micropollutants, including 12 anionic PFASs at environmentally relevant concentrations[27]. These functional groups facilitate the adsorption of anionic PFASs, including short-chain and branched PFASs, which typically exhibit weaker host-guest interactions with β-CD. This improved adsorption performance was attributed to complementary electrostatic interactions between the adsorbent and targeted pollutants. Wang et al. reported the incorporation of amino groups into β-CD to synthesize crosslinked polymers (β-CD-COFs) of different sizes to improve the binding sites for the rapid removal and high adsorption capacity for many anionic PFASs, including short-chain derivatives[17]. The synthesized β-CD-COFs exhibited rapid kinetics and high adsorption capacities (0.33–1.51 mmol g^{-1}) for four short- and long-chain PFASs, which were significantly better than traditional resins and ACs. Till now, numerous studies have reported the high adsorption capacity of β-CD polymers for PFASs. However, the impacts of different water parameters and wastewater containing different inorganic and organic impurities in real wastewater systems still need to be investigated. Additionally, these polymers raise fundamental questions about their significant adsorption capacity and kinetic rate for short-chain PFASs and the relative role of amines in crosslinking with β-CD and providing binding sites for PFASs adsorption. Furthermore, the relative significance of the host-guest interactions within the cavity of the β-CD and electrostatic interactions from the amino groups in capturing PFASs is unclear, particularly in post-polymerization-modified polymers.

In this study, a tripodal crosslinker containing three amine groups was synthesized via the condensation reaction between tris(2-aminoethyl)amine (TREN) and pentafluorobenzaldehyde under anhydrous conditions, followed by the reduction of imines using sodium borohydride. The crosslinker was then incorporated with β-CD through the nucleophilic aromatic substitution reaction to obtain a three-amine-containing β-CD-TriPod polymeric adsorbent. This adsorbent was evaluated in terms of its performance to adsorb nine PFASs, including short-chain variants. The adsorbent was also investigated for the synergetic combination of electrostatic and host-guest inclusion interactions. A series of batch adsorption parameters, including pH, contact time, variation of initial concentration, regeneration, and reusability, were systematically investigated to achieve optimum results for both selective long-chain PFOS and its short-chain replacement, i.e., PFBS. Lastly, the adsorption performance of the β-CD-TriPod adsorbent was investigated in the presence of natural organic matters (NOM) and in real industrial wastewater to demonstrate its superior capability in treating water contaminated with both short- and long-chain PFASs.

Results and discussion

Characterizations of adsorbent

The β-CD-TriPod polymer was synthesized using nucleophilic aromatic substitution reaction between the TriPod-crosslinker and β-CD (Fig. 1). Fourier-transform infrared spectroscopy (FTIR), nuclear magnetic resonance (NMR), and liquid chromatography-mass spectrometry (LC-MS) were utilized to confirm the successful synthesis and presence of various functional groups. The FTIR data of β-CD, TriPod-crosslinker, and β-CD-TriPod polymeric adsorbent are shown in Fig. 2a. The TriPod crosslinker, consisting of three aromatic groups, exhibited distinct vibrational modes at 3351 cm^{-1}, 2839 cm^{-1}, 1654 cm^{-1}, 1494 cm^{-1}, and 1154 cm^{-1}, corresponding to N−H stretching, aliphatic N−C stretching, N−H bending, aromatic C=C stretching, and aromatic C−F stretching, respectively. In the β-CD-TriPod polymer, strong bands appeared at 3382 cm^{-1}, 2924 cm^{-1}, and 1024 cm^{-1}, corresponding to O−H stretching, aliphatic C−H stretching, and C−O stretching of the β-CD moiety, respectively. These bands, along with the vibrational peaks from the TriPod-crosslinker, confirm the successful formation of the polymeric network adsorbent. Table S2 summarizes the lists of different vibrational modes of β-CD and TriPod-crosslinker observed in the β-CD-TriPod polymeric network. The H1 NMR spectrum (600 MHz, $CDCl_3$) of the synthesized crosslinker exhibited signals at δ 1.63 (s, 3H, **NH**), 2.49 (t, 6H, N **CH2**), 2.457 (t, 6H, NCH_2 **CH_2**), and 3.88 (s, 6H, Ar **CH_2**), confirming the successful incorporation of β-CD onto TriPod-crosslinker (Fig. S1). The MS with an electrospray ionization source (ESI) of the synthesized tripodal crosslinker exhibited prominent peaks at *m/z* 687.1 and 688, supporting the formation of a highly pure crosslinker (Fig. S2). These FTIR, NMR, and MS data confirm the formation of highly pure Tripod-crosslinker and β-CD-TriPod adsorbent. The thermogravimetric analysis (TGA) data for the β-CD-TriPod polymer are presented in Fig. 2b, demonstrating a three-step weight loss process, after which approximately 25% of the weight remained at 600 °C. The first step of weight loss was observed up to 65 °C due to moisture loss, the second step of weight loss between 220–390 °C was probably due to thermal decomposition of β-CD and TriPod polymer, and the third step of weight loss was due to breakdown of the carbon framework[30]. The morphology of the prepared β-CD-TriPod adsorbent was investigated using field emission scanning electron microscopy (FESEM) (Fig. 2c, d), revealing a rigid and porous type of network. This type of structure is beneficial in the adsorption of PFASs, as previously reported[25]. The elemental mapping of β-CD-TriPod polymer is shown in Fig. S3, revealing a uniform distribution of carbon (C), oxygen (O), nitrogen (N), and fluorine (F). Energy-dispersive X-ray spectroscopy (EDS) attached to FESEM, quantifies the elemental composition in atomic percentages (at%), revealing C: 64.87%, N: 7.91%, O: 21.40%, and F: 5.82%. This elemental mapping and composition support successful crosslinking via nucleophilic aromatic substitution reaction between the β-CD macromolecule and the TriPod-crosslinker, due to the presence of the O element with N and F.

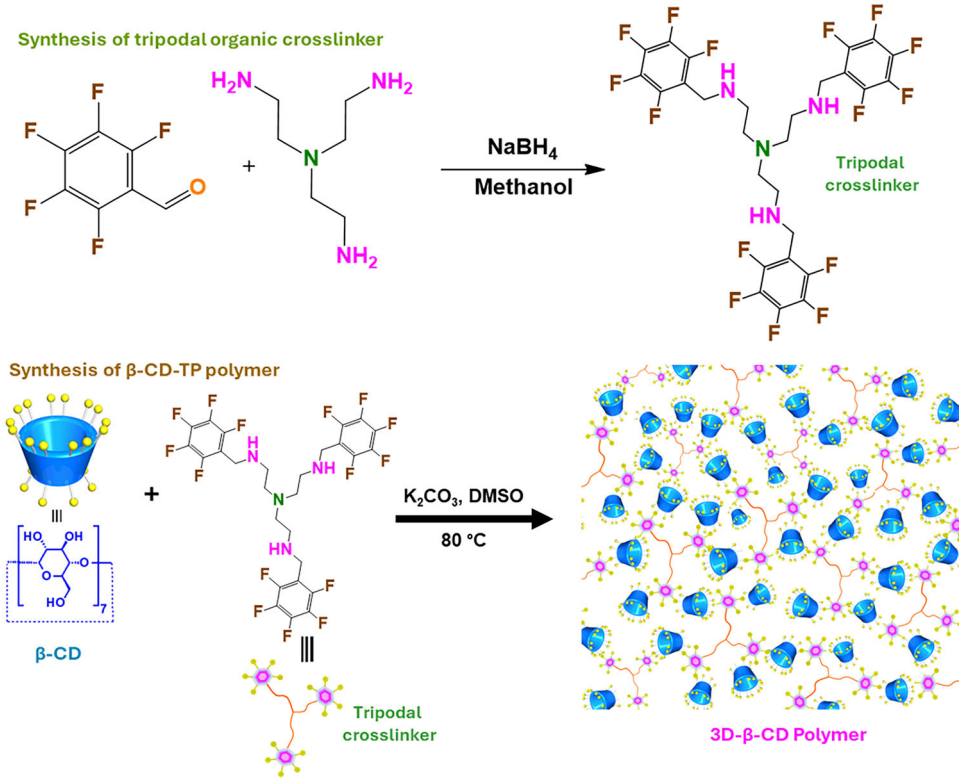

Fig. 1 | Schematic synthesis of β-CD crosslinked with tripodal amine (β-CD-TriPod) polymer.

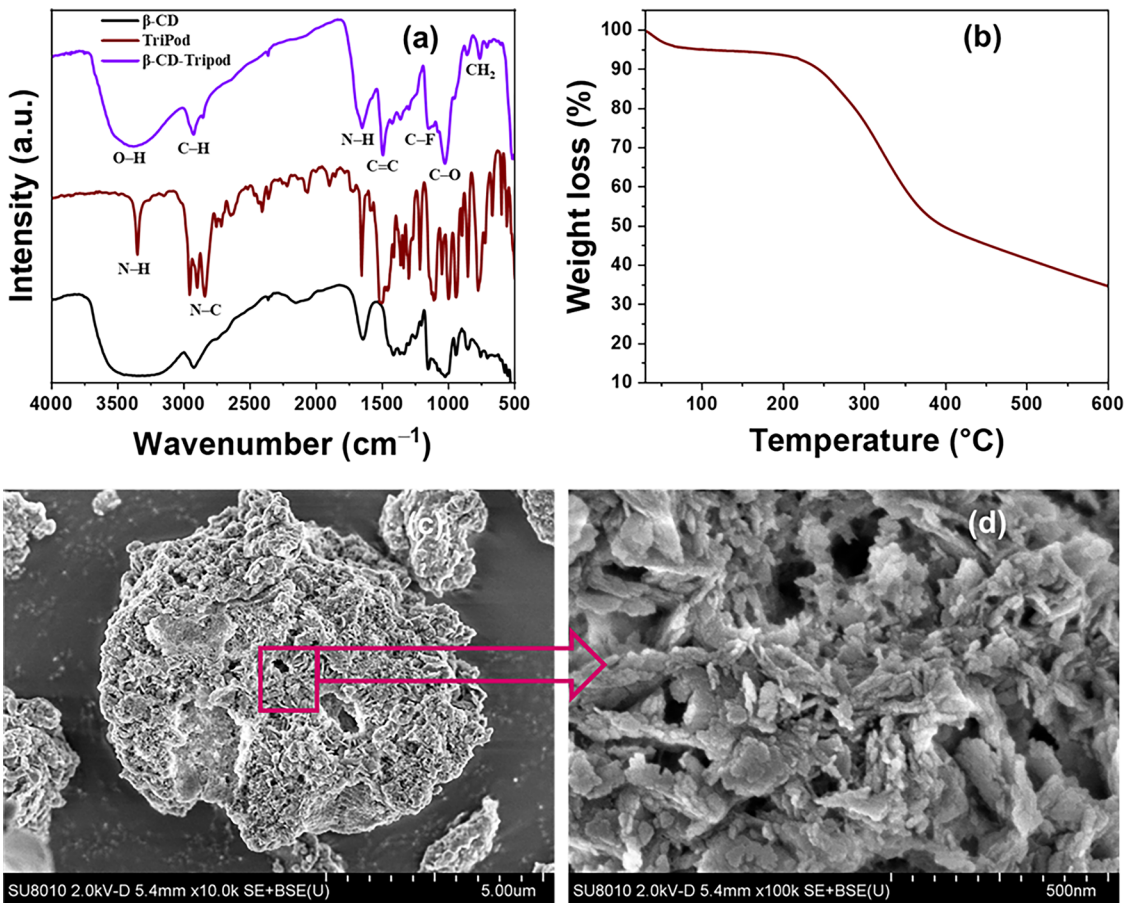

Fig. 2 | Characterization of β-CD-TriPod polymer synthesized in this study. FTIR spectra (**a**), TGA profile (**b**), and FESEM images at lower and higher magnification (**c**, **d**) of β-CD-TriPod polymer.

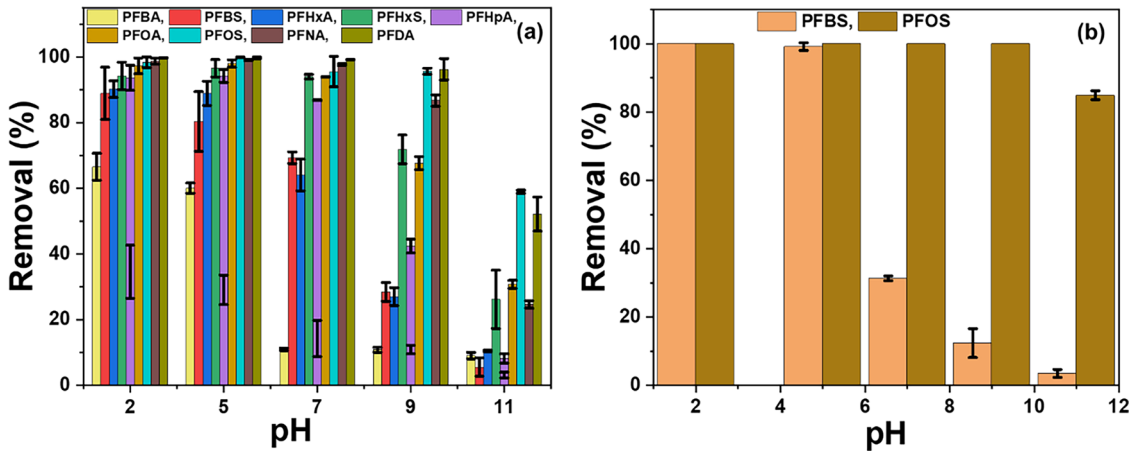

Fig. 3 | Effects of pH on removal of PFASs by β-CD-TriPod polymer. Effect of pH on the removal efficiency of nine PFASs (**a**) and individually with PFBS and PFOS (**b**) ([PFASs]$_0$ = 1 μg L^{-1}, adsorbent dose: 10 mg L^{-1}, pH range: 2–11). Error bars indicate the standard deviation.

pH effect

Solution pH is a critical parameter in the removal of PFASs, therefore, we explored the effect of pH on the adsorption of nine PFASs in mixture form, as well as individually with PFBS and PFOS on the β-CD-TriPod polymer (Fig. 3a, b). The data indicate that the adsorption efficiency for both short- and long-chain PFASs was significantly high at pH 2, 5, and 7, but substantially lower at pH 11. At pH 2, the removal efficiencies were 66.50%, 88.90%, 90.20%, 94.30%, 93.60%, 97.30%, 98.50%, 98.70%, and 99.70%, and decreased to remain 10.80%, 28.50%, 27%, 71.80%, 42.40%, 67.60%, 95.70%. 86.70%, and 96.20% at pH 9, corresponding to PFBA, PFBS, PFHxA, PFHxS, PFHpA, PFOA, PFOS, PFNA, and PFDA, respectively. Among these, the adsorption efficiencies for long-chain PFASs, including PFHxS, PFHpA, PFOA, PFOS, PFNA, and PFDA, remained relatively stable at pH 5 and only slightly changed with increasing pH at 7. This trend indicates a strong affinity of the β-CD-TriPod polymer loaded with amino groups for different PFASs under acidic conditions. This observed decrease in removal efficiency with increasing pH can be explained by the surface chemistry and charge properties of β-CD-TriPod polymeric adsorbent and PFASs speciation. Based on the estimated pK_a values, which are negative or less positive (Table S3), the PFASs examined in this study exhibit anionic characteristics within the tested pH range, and the amino groups incorporated into β-CD showed a zeta potential of 1.45 ± 0.70 at pH 7. Therefore, these groups were protonated in acidic solutions and facilitated electrostatic interactions for the adsorption of PFASs. At lower pH levels, the higher positive zeta potential provides a strong electrostatic interaction, resulting in higher removal efficiencies. However, as the pH increases (in basic solutions), the β-CD-TriPod polymer surface became more negative due to the negative zeta potential, and the weakly basic functional groups (−NH_2) in the crosslinker turned into less positive surface (i.e., deprotonated), leading to electrostatic repulsion with the PFASs, and a consequent decrement in removal efficiencies was observed[4]. In the case of individual PFOS and PFBS, almost complete removal efficiencies were achieved at pHs 3 and 5, which were sustained up to pH 9 for PFOS, whereas, decreased to reach 12.40% in the case of PFBS at pH 9. Previous studies reported that the hydrophobic interactions between the perfluorinated chains and β-CD play a significant role in the adsorption of linear, long-chain PFASs, along with electrostatic interactions, therefore, 100% removal efficiency was achieved for PFOS. However, short-chain and branched PFASs were primarily adsorbed by electrostatic interactions, which decreased due to the deprotonation of amino groups, therefore, a sudden decrement in the removal efficiency of PFBS after pH 5.0 was observed (Fig. 3). These findings highlight the critical role of electrostatic interactions in the adsorption of short-chain PFASs, while both electrostatic and hydrophobic (host-guest) interactions role in the adsorption of long-chain PFASs. Figure S4 presents the data of nine PFASs on β-CD-TriPod polymer at pH 2 and 5 only. Overall, PFASs are frequently present in some acidic wastewater (low pH conditions), therefore, the prepared β-CD-TriPod can effectively remove the PFASs, including short-chain PFASs, which are traditionally challenging to adsorb from water with conventional adsorbents such as ACs, GAC, and PAC.

Contact time effect and adsorption kinetics

The adsorption performance of the synthesized β-CD-TriPod polymer was evaluated to describe the adsorption kinetics and equilibrium for nine PFASs, both in a mixture and individually with PFBS and PFOS, at environmentally relevant concentration (1 μg L^{-1}). The results of the kinetic experiments are presented in Fig. 4a, b, and their short time-interval data are given in Figs. S5 and S6, including the average data and standard deviation (%). Also, Fig. S7 showed the adsorption equilibrium of nine PFASs under short intervals at lower concentrations. The data indicate the rapid adsorption equilibrium, which was achieved within 2 min, with removal efficiencies of >99% for the targeted anionic PFASs, including both perfluorinated sulfonates (PFSA) and carboxylates (PFCA) with chain lengths ranging from 4 to 10, except for PFBA, which could attain the equilibrium in 15 min. Additionally, the β-CD-TriPod polymer showed excellent adsorption affinity for both short-chain PFBS and long-chain PFOS individually at 1 μg L^{-1}, as shown in Fig. 4b, with removal efficiencies of <99.50% within 2 min. This adsorption equilibrium time is significantly shorter than those previously reported for conventional adsorbents, including various types of ACs, GAC, and PAC (Table S5), confirming the potential of the prepared β-CD-TriPod polymer in the removal of anionic PFASs with an extremely faster rate. An interesting point was noted for PFASs with the same carbon number (C_4); the removal efficiency was higher (100%) for PFBS compared to PFBA (75.45%). This difference was attributed to the presence of the sulfonic head group in PFBS, which has a higher electron density to interact in a better way with existing protonated amino groups in the β-CD-TriPod adsorbent[17]. Overall, the results obtained from mixture or individual PFASs at environmentally relevant concentrations confirm that the β-CD-TriPod adsorbent can effectively adsorb the target PFASs to reduce their residual concentration below 25 ng L^{-1}, which is significantly lower than the health advisory levels of 70 ng g^{-1} set by the U.S. EPA for PFOS and PFOA. Earlier studies have also reported that the longer-chain PFASs were adsorbed more easily than shorter-chain PFASs, and the removal efficiencies were decreased with decreasing tail lengths of PFASs. This trend was attributed to the stability of inclusion complex formation, which depends on the size of the potential guest (tail of PFASs) that fits into the β-CD cavity[17]. The stability constants calculated for β-CD complexes were increased with increasing PFAS chain length due to stronger hydrophobic interactions. A similar trend was also observed in the study of solution-based titration between β-CD and PFASs[28]. Also, the long-chain PFASs exhibit more hydrophobicity, which enhances their tendency to transfer from the aqueous solution to the solid adsorbents,

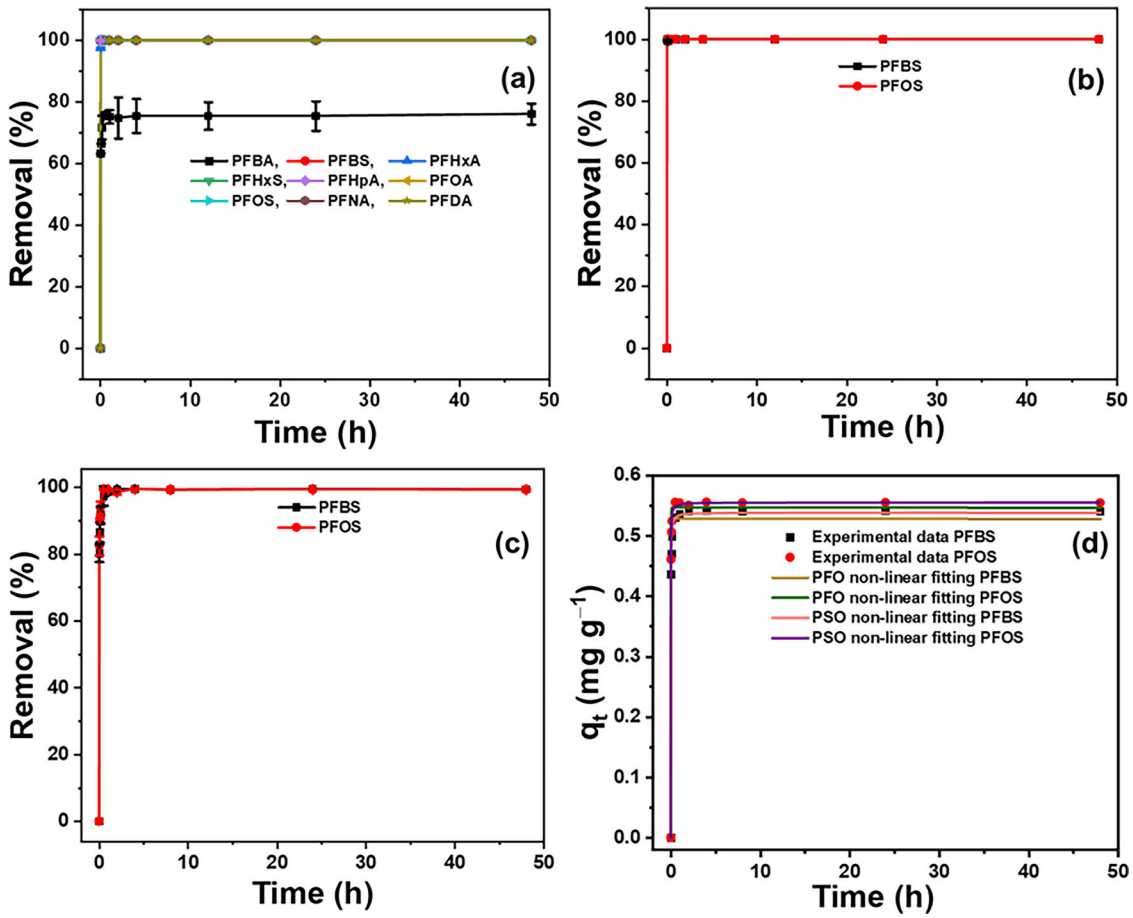

Fig. 4 | Application of PFO and PSO models for kinetics of PFAS adsorption to β-CD-TriPod polymer. Kinetics of adsorption of nine PFASs to β-CD-TriPod (**a**, **c**) and individually with PFBS and PFOS (**b**), and non-linear fits of adsorption data to PFO and PSO kinetics (**d**). $[PFASs]_0$: 1 μg L^{-1} for (**a**, **b**) and 200 μg L^{-1} for (**c**); adsorbent dose: 10 mg L^{-1} for (**a**, **b**) and 400 mg L^{-1} for (**c**); pH 5.0 for (**a**–**c**). Error bars = standard deviation of three experiments.

Table 1 | PFO and PSO non-linear fitting parameters for PFBS and PFOS onto β-CD-TP polymer

System	PFO				PSO		
	$q_{e,exp}$ (mg g^{-1})	$q_{e,cal}$ (mg g^{-1})	k_1 (h^{-1})	R^2	$q_{e,exp}$ (mg g^{-1})	k_2 (g mg^{-1}·h^{-1})	R^2
PFBS	0.540	0.530 ± 0.007	55.40 ± 7.70	0.982	0.540 ± 0.003	210.50 ± 22.10	0.997
PFOS	0.554	0.550 ± 0.004	59.80 ± 6.10	0.991	0.550 ± 0.002	277.10 ± 16.10	0.999

Dose = 200 mg L^{-1}, initial concentration: 200 μg L^{-1} and pH: 2.2.

thereby increasing adsorption affinity. In such of mechanism, the long-chain PFASs interact with protonated amine groups via electrostatic interactions, as well as hydrophobic interactions within the β-CD cavity, while the short-chain PFASs, such as PFBA and PFBS, experience lower binding efficiency due to reduced van der Waals interactions within the interior cavity of the β-CD. Moreover, the long-chain PFSAs may interact more effectively with the relatively wider interior of β-CD-TriPod, as their molecular structure allows for better integration within the adsorbent's porous network, as observed in FESEM, further leading the engagement in removal efficiency.

The adsorption kinetics and equilibrium were also investigated individually with PFBS and PFOS at higher concentrations (200 μg L^{-1}), which is generally higher than those reported in contaminated waters, using 400 mg L^{-1} adsorbent concentration. The results are presented in Figs. 4c and S8, demonstrating rapid uptake of both PFBS and PFOS, with removal efficiencies of 80.30% and 83.50% within 2 min, and 97.40% and 99.40% within 30 min, respectively.

Two well-known adsorption kinetics models, i.e., pseudo-first-order (PFO) and pseudo-second-order (PSO), were applied non-linearly to the kinetic data to describe the adsorption rate control and type of adsorption. The adsorption kinetics model predictions and their corresponding experimental data are shown in Fig. 4d and Table 1, respectively. The results indicate that the adsorption behavior of PFASs onto β-CD-TriPod is described well with both PFO and PSO models, as indicated by high coefficients of determination ($R^2 > 0.987$). This high R^2 value for both models implied that PFASs adsorption onto β-CD-TriPod was not only affected by physical adsorption, but also by chemical adsorption. The rate constant (k_2) values were determined to be 210.50 ± 22.10 and 277.10 ± 16.10 g mg^{-1} h^{-1} for PFBS and PFOS, respectively, indicating much faster adsorption compared to the previously reported different types of GAC, PAC, resin, and other adsorbents (Table S5). The higher k_2 value for PFOS compared to PFBS again confirms the important role of hydrophobic interaction along with electrostatic interaction in the adsorption of long-chain PFASs[19].

Adsorption isotherm

We constructed the adsorption isotherm for PFBS and PFOS on β-CD-TriPod adsorbent to evaluate the adsorption capacity and mechanism. The

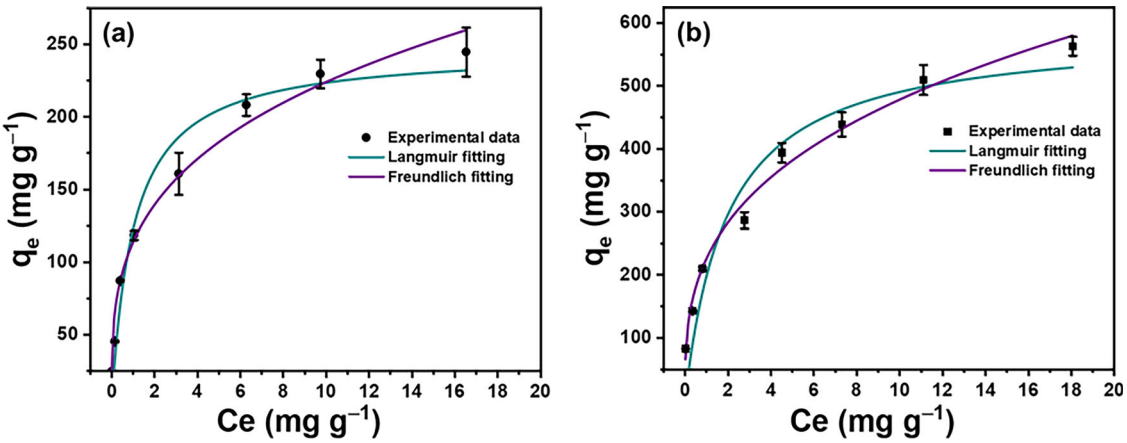

Fig. 5 | Isotherm study of adsorption of PFBS and PFOS onto β-CD-TriPod polymer. Non-linear isotherms fits for adsorption of PFBS (**a**) and PFOS (**b**) onto β-CD-TriPod polymer. ($[PFBS]_0$ range: 1–25 mg L^{-1}, ($[PFOS]_0$ range: 3–40 mg L^{-1}, adsorbent dose: 200 mg L^{-1}, pH 3.0. Error bars indicate the standard deviation.

Table 2 | Fitting results of Langmuir and the Freundlich isotherms applied for the adsorption of PFBS and PFOS on β-CD-TP polymer

Isotherms fitting	Parameters	PFASs	
		PFBS	PFOS
Langmuir	$q_{m,exp}$ (mg g^{-1})	245 ± 17	563 ± 15
	$q_{m,\ cal}$ (mg g^{-1})	246 ± 15	587 ± 55
	K_L (L mg^{-1})	0.31 ± 0.18	0.98 ± 0.26
	R^2	0.959	0.927
Freundlich	K_F (mg g^{-1}) (L mg^{-1})$^{1/n}$	113 ± 6	226 ± 10
	N	3.39 ± 0.26	3.06 ± 0.19
	R^2	0.983	0.988

Adsorbent dose = 200 mg L^{-1}, contact time: 360 min, and pH: 2.2.

initial adsorption dose was chosen as 200 mg L^{-1}, while the initial concentration range for PFBS and PFOS was chosen as 1–25 mg L^{-1} and 3–40 mg L^{-1}, respectively. Two well-known isotherm models, Langmuir and Freundlich, were applied non-linearly to the adsorption data (Fig. 5a, b), and the model parameters are presented in Table 2. The Langmuir model fitting ($R^2 > 0.927$) provides the maximum adsorption capacities: 246.20 ± 14.80 mg g^{-1} for PFBS and 587.10 ± 54.50 mg g^{-1} for PFOS, along with the affinity coefficients (K_L) 0.310 ± 0.180 L mg^{-1} and 0.980 ± 0.260 L mg^{-1}, respectively. Additionally, the Freundlich model was also fitted well ($R^2 > 0.983$) to the adsorption data, with nonlinearity fitting (n) values calculated to be more than 3.0 for both PFBS and PFOS, suggesting the favorable adsorption of PFASs onto β-CD-TriPod adsorbent. The Langmuir adsorption affinity values (K_L) obtained for β-CD-TriPod adsorbent are at least thirteen times higher than those of GAC (0.0758) and PAC (0.1070)[31,32]. In short, the adsorption capacity and affinity values of β-CD-TriPod are significantly superior to those previously reported in studies performed with different types of adsorbents, including β-CD-based polymeric adsorbents (Table S5)[33]. Additionally, it was observed that the β-CD-TriPod adsorbent showed five times higher affinity (4.9×10^5 M^{-1}) and more than two times adsorption capacity (587 mg g^{-1}) for PFOS compared to PFBS (adsorption affinity: 9.3×10^4 M^{-1} and capacity: 246 mg g^{-1}). This data supports the synergetic effects of the hydrophobic cavity of β-CD and amine groups within β-CD-TriPod adsorbent for the binding of PFOS via host-guest inclusion interactions and electrostatic interactions, respectively. Earlier, Ji et al. reported the binding capacity of imine-linked 2D-COFs functionalized with amine functional groups for GenX adsorption and found that the partial amine incorporation resulted in the highest adsorption rate and capacity owing to the synergetic effect of the polar amine groups and hydrophobic surfaces, which collectively enhanced binding sites availability for GenX adsorption[34].

NOM effect

NOM is another important factor that significantly affects the pollutants distribution in water and the adsorption efficiency of ACs due to providing the fouling nature, while it is less sensitive towards β-CD-based polymers[26]. Therefore, the adsorption of nine PFASs was evaluated in the presence of humic acid (HA), an important component of NOM. The experiment was performed by taking a 20 mg L^{-1} concentration of HA in a water matrix with an initial concentration of each PFAS (1 µg L^{-1}) and β-CD-TriPod (10 mg L^{-1}) polymer at pH 5.0. The results are presented in Fig. 6a, demonstrating that the presence of HA slightly suppressed the adsorption of short-chain PFASs, whereas the adsorption of long-chain PFASs was not significantly inhibited in water. This selective interference might be due to the higher binding affinity of β-CD-TriPod towards long-chain PFAS, which preferably occupy adsorption sites over short-chain PFASs, and these interferences are caused due to driving adsorption inhibition by the presence of NOM[35]. Nevertheless, these findings clearly confirm the superior fouling resistance and significant selectivity of β-CD-TriPod towards PFASs removal.

Regeneration and stability

Regeneration and reusability are crucial parameters for the economic and practical perspectives for an adsorbent in wastewater treatment. Therefore, regeneration and reuse experiments were conducted up to five consecutive adsorption-desorption cycles by adding 50 mg β-CD-TriPod to 100 mL of 200 µg L^{-1} PFBS and PFOS individually at pH 5.0, while desorption performance was investigated in methanol. The obtained results are presented in Fig. 6b, indicating no significant loss in efficiency for both PFBS and PFOS, and the desorbed amount of them was almost equal to the adsorbed amount. The adsorption efficiencies of β-CD-TriPod for PFBS and PFOS were obtained as more than 99% in the first cycle and dropped by 96% and 94%, respectively, after the fifth adsorption cycle. The desorbed amount was more than 97% in the first cycle, which was sustained at around 93% and 96% after the fifth desorption cycle for PFBS and PFOS, respectively. An additional regeneration experiment was performed using a mixture of PFBA, PFBS, PFOA, and PFOS under the same experimental conditions, and the results are shown in Fig. S9. The data indicate almost stable regeneration efficiencies in the case of long-chain PFASs (PFOA and PFOS) for up to five cycles, while in the case of short-chain PFASs (PFBA and PFBS), a significant reduction in adsorption efficiency was observed after the first regeneration cycle, which remained relatively stable during the subsequent four cycles. The adsorption efficiencies for PFBA, PFBS, PFOA, and PFOS were 63.50%, 94%, 97%, and 99.10% in the first cycle, and then

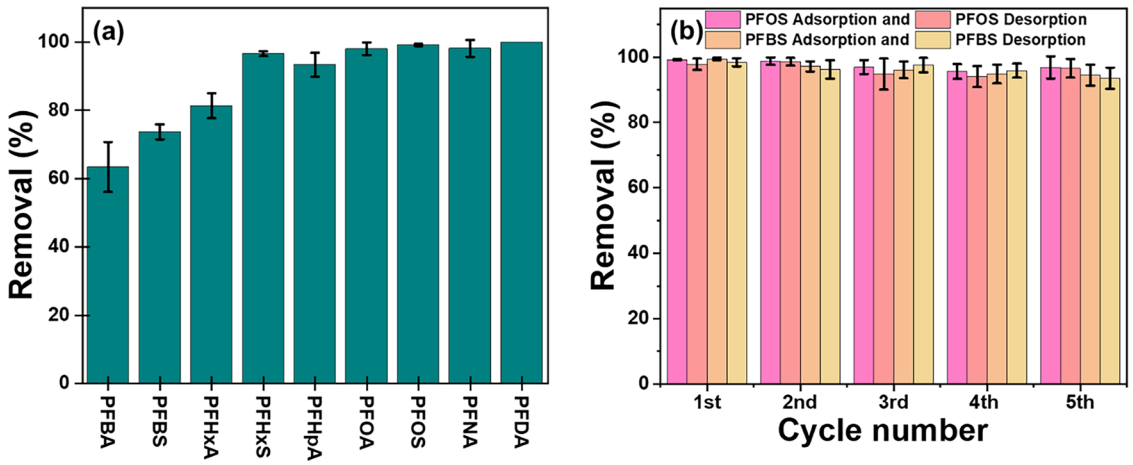

Fig. 6 | Usability of β-CD-TriPod polymer in removing PFASs in water. Effect of HA on the adsorption of nine PFASs onto β-CD-TriPod. ($[PFASs]_0$ = 1 μg L^{-1}, β-CD-TriPod dose: 10 mg L^{-1}, pH 5.0) (**a**) and adsorption and desorption efficiencies of β-CD-TriPod after regeneration and reuse for PFOS and PFBS. For adsorption: $[PFASs]_0$ = 200 μg L^{-1}, β-CD-TriPod dose: 500 mg L^{-1}. For desorption: β-CD-TriPod used was suspended in 50 mL MeOH for 24 h (**b**). Error bars indicate the standard deviation.

dropped to 37%, 63.50%, 85.90%, and 93.70% after five cycles, respectively. The reduction in efficiencies towards short-chain PFASs is likely due to their less hydrophobic nature, as less hydrophobic molecules have the tendency to release at a faster rate from the adsorbent. After the first cycle, the long-chain PFAS molecules compete more effectively for the remaining adsorption sites in the form of amine groups and hydrophobic cavities, and due to their higher hydrophobicity, they were absorbed before the short-chain PFASs. To investigate the faster desorption, an additional experiment was performed to assess the rapid desorption of PFOS from β-CD-TriPod with methanol in 10 min, and the results are shown in Fig. S10. The data clearly suggest the complete desorption of PFOS from β-CD-TriPod adsorbent, confirming its potential as a rapid and effective reusable adsorbent in comparison to ACs such as GACs and PACs[36].

Adsorption performance in real wastewater

In the next step, we have examined the performance of β-CD-TriPod in real wastewater, considering the presence of different inorganic anions, cations, and other organic pollutants that could potentially inhibit the efficiency of the adsorbent. The different physical characteristics of the effluent are shown in Table S4. The wastewater was collected from a treatment plant, Seoul, South Korea, with an in-situ pH of 12.6. This wastewater contained no detectable background level of any PFASs, which were used in this study. Prior to the experiments, the collected wastewater was filtered using Whatman filter paper and then adjusted to pH 5.0, as adjusted during the pH effect study. The initial concentrations of nine PFASs were used as 1 μg L^{-1} for each and 10 mg L^{-1} adsorbent solution for the experiment. Similar adsorption tests were performed with previously reported GAC, β-CD-TFN, and β-CD-DFB adsorbents on an equivalent mass basis to show the comparison in results (Fig. 7)[37]. The removal efficiencies of the β-CD-TriPod adsorbent were found to be 55.30%, 79%, 85.10%, 99.30%, 95.90%, 97.70%, 100%, 99.90%, and 99.70% for PFBA, PFBS, PFHpA, PFHxA, PFOA, PFHxS, PFOS, PFNA, and PFDA, respectively. These values were significantly higher than those of GAC, which showed the removal efficiencies of 13.80%, 25.60%, 19.70%, 35.30%, 24.10%, 37.70%, 87.30%, 82.90%, and 96.50%, respectively, for the same PFASs. The adsorption efficiencies of β-CD-TFN adsorbent (surface area 263 m^2 L^{-1}) were almost negligible, remaining below 3.5% for all nine PFASs, despite its previously reported effectiveness in removing various other organic micropollutants[25]. Lastly, equilibrium removal efficiency was compared with β-CD-DFB adsorbent, a known effective and non-fouling adsorbent for long-chain PFASs, and the values were found to be 4.80%, 6.50%, 10.80%, 55.60%, 42.20%, 81.90%, 86.90% 83.30%, and 91.90% for PFBA, PFBS, PFHpA, PFHxA, PFOA, PFHxS, PFOS, PFNA, and PFDA, respectively.

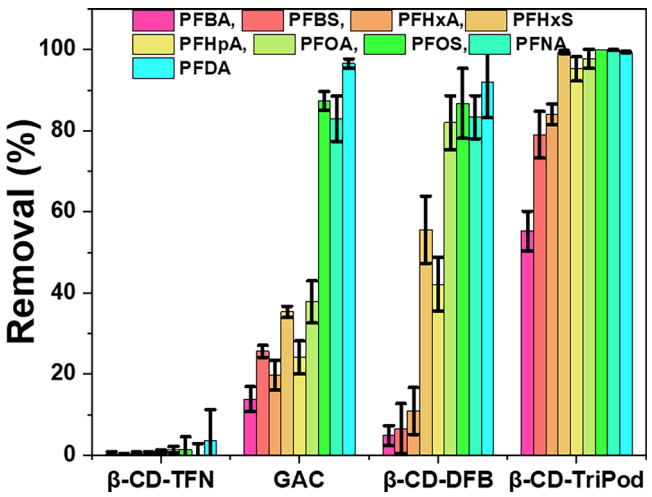

Fig. 7 | Removal efficiency of the nine PFASs from filtered WW onto equal mass concentrations of GAC, β-CD-TFN, β-CD-DFB, and β-CD-TriPod polymer adsorbent. ($[PFASs]_0$ = 1 μg L^{-1}, adsorbent dose: 10 mg L^{-1}, pH 5.0). Error bars indicate the standard deviation.

Overall, the adsorption of PFASs onto β-CD-TriPod adsorbent was not significantly inhibited by the complexity of the wastewater matrix, and the remaining concentration of PFASs, particularly for PFHpA, PFHxS, PFOA, PFOS, PFNA, and PFDA, was maintained below 50 ng L^{-1}, which is significantly below the drinking water standard of 70 ng L^{-1} established by the Ministry of Environment, South Korea[38]. These collective findings suggest that β-CD-TriPod adsorbent exhibits exceptional potential as a highly effective adsorbent for the removal of a wide range of PFASs from real wastewater.

Adsorption mechanism

Lastly, the adsorption mechanism was investigated to examine "how long-chain and short-chain PFASs interact with β-CD-TriPod adsorbent." For PFASs adsorption, both electrostatic and hydrophobic interactions were the dominating attractions, as discussed in the previous sections. For this purpose, an adsorption equilibrium experiment was performed individually with PFBS and PFOS. The adsorbate and adsorbent concentrations were chosen as 20 mg L^{-1} and 400 mg L^{-1} at pH 5, respectively. After equilibrium, the adsorbent was filtered and dried for elemental mapping, composition,

and FTIR analysis to investigate the elemental distribution and compositions after PFASs adsorption and changes in the functional groups, respectively. The elemental mapping and distribution are shown in Figs. S11 and S12, indicating the addition of uniformly distributed colorful elemental signal spots of sulfur (S) along with other elements, confirming the adsorption of PFBS and PFOS on the surface of β-CD-TriPod adsorbent. The elemental compositions of C, N, O, F, and S elements of β-CD-TriPod were found to be in at% as 66.61%, 7.0%, 20.80%, 5.33%, and 0.25% in case of the PFBS adsorption (Fig. S13), and 66.04%, 7.90%, 18.58%, 6.81%, and 0.67% in case of PFOS adsorption (Fig. S14), respectively. In elemental compositions, it is noticeable that the elemental ratio of "S" in PFOS and PFBS adsorption (PFOS/PFBS) is nearly equal to the ratio of their adsorption capacities calculated during the isotherm analysis, further supporting the synergetic effects of amines and hydrophobic β-CD cavities in β-CD-TriPod adsorbent in the binding of PFOS via both electrostatic and host-guest interactions. In support of the electrostatic interactions, FTIR data were compared before and after the adsorption (Fig. S15), indicating the absence of any changes in the peak positions, except for a slight shifting of the amine group from 3351 cm^{-1} to 3383 cm^{-1} and 3391 cm^{-1} after PFBS and PFOS adsorption, respectively. Additionally, a new S=O peak appeared at 1216 cm^{-1} in the case of PFBS adsorption, compared to 1242 cm^{-1} in PFOS adsorption, confirming that PFBS was adsorbed only by electrostatic interactions, whereas PFOS was adsorbed via hydrophobic interactions within the β-CD cavity along with electrostatic interactions. Previously, Wang et al. reported similar types of electrostatic interactions with amine groups in the case of short-chain PFBS adsorption, while both electrostatic and hydrophobic interactions in the case of long-chain PFOS adsorption onto amine-containing β-CD COF using the electrostatic potential (ESP) calculation process[17]. As discussed in the kinetics and isotherm sections, long-chain PFASs have a higher tendency to adsorb via electron-deficient β-CD's cavity than short-chain; therefore, PFOS could be adsorbed via hydrophobic interaction along with electrostatic interactions, whereas PFBS could be absorbed only via electrostatic interactions.

A detailed comparison of the adsorption kinetics and capacities of the various adsorbents is shown in Table S5. Yu et al. previously reported the rapid adsorption of PFOS onto GAC and PAC large surface area and suitable porosity to form micelles via hydrophobic interactions[39]. Apart from it, the β-CD-TriPod adsorbent clearly demonstrates superiority in terms of adsorption kinetics, capacity, and affinity, and this is likely due to the introduction of additional electrostatic interactions within the β-CD network, which is the key designing principle to enhance the effectiveness in removing both short-chain and long-chain PFASs, distinguishing it as an advanced adsorbent solution.

In summary, this study reported the successful synthesis of β-CD-based adsorbent with a tripodal crosslinker with three amino-groups via nucleophilic aromatic substitution reaction and systematic evaluation of its efficiency for the removal of short and long-chain PFASs at different concentration ranges from water. The pH results presented a strong affinity of β-CD-TriPod polymer towards PFASs in acidic conditions. The rate constants (k_2) for the PSO kinetics model were 210.50 ± 22.10 and 277.10 ± 16.10 g mg^{-1} h^{-1} for PFBS and PFOS, respectively, demonstrating a rapid adsorption in comparison with previously reported different types of GAC, PAC, and other adsorbents. The adsorption isotherm results provided Langmuir adsorption capacities as 246.20 ± 14.80 mg g^{-1} for PFBS and 587.10 ± 54.50 mg g^{-1} for PFOS, alongside affinity coefficients (K_L) 0.31 ± 0.18 and 0.98 ± 0.26 L mg^{-1}, respectively, emphasizing the synergistic combination of well-defined electrostatic interactions and host-guest interactions as an ideal design criterion for complete PFASs removal. The adsorption-desorption process, conducted by simple washing with methanol, achieved over 94% adsorption efficiency after the fifth cycle, confirming its relatively high stability and reusability. In the real wastewater matrix, efficiency was not significantly affected by other organic and inorganic contaminants. The adsorption mechanism confirms the role of electrostatic interactions in the adsorption of short-chain PFASs, whereas long-chain PFASs removal is obtained via both electrostatic and hydrophobic interactions. Overall, the results suggest that the β-CD-TriPod polymer is an effective and promising candidate for PFASs remediation, and future studies will focus on the investigation of zwitterionic, non-ionic, and cationic PFASs removal more deeply and their interactions within complex wastewater treatment systems.

Methods

Chemicals and reagents

Detailed information regarding the chemicals and reagents used in this study is provided in Supplementary Information (Text SI-1).

Synthesis of β-CD-TriPod adsorbent

The β-CD-based adsorbent crosslinked with three amino groups containing TriPod crosslinker was prepared in two steps:

In the first step, a tripodal monomer crosslinker containing trifunctional amine was prepared by condensing the TREN with pentafluorobenzaldehyde under anhydrous conditions, followed by reduction to the imine group using sodium borohydride[40]. In the second step, nucleophilic aromatic substitution of the tripodal crosslinker was performed with β-CD to obtain a three amine-containing β-CD-TriPod crosslinked polymer as previously reported[41], as illustrated in Fig. 1. To optimize the polymer yield, several synthesis parameters were systematically evaluated, including the ratio of β-CD to the tripodal crosslinker, solvent concentration, base identity, and base amount, as detailed in Table S1. A detailed synthesis procedure is provided in SI.

Synthesis of tripodal monomer crosslinker. In the first step, a tripodal crosslinker was prepared according to a previously reported method[40]. To a solution of pentafluorobenzaldehyde (1.764 g, 9 mmol, 3 equiv) in 50 mL of dry methanol, a solution of TREN (0.448 g, 3 mmol, 1 equiv) in 30 mL of dry methanol was added dropwise over 30 min under nitrogen at room temperature. After stirring for 24 h, the solution was cooled in an ice bath, and a small portion of excess $NaBH_4$ (0.454 g, 12 mmol, 4 equiv) was added. The solution was stirred for another 4 h and then refluxed for 2 h. Methanol was removed under reduced pressure, and the residue was extracted with chloroform and water. The collected organic layers were dried with anhydrous sodium sulfate and evaporated under reduced pressure. Lastly, the compound was purified by column chromatography using dichloromethane/methanol (9.5/0.5) as the eluent to obtain a light-yellow solid. The FTIR data provide peaks situated at 3351 cm^{-1}, 2839 cm^{-1}, 1654 cm^{-1}, 1494 cm^{-1}, and 1154 cm^{-1} corresponding to N−H stretching, aliphatic N−C stretching, N−H bending, aromatic C=C stretching, and aromatic C−F stretching, respectively. The 1H NMR (600 MHz, $CDCl_3$): δ 1.63 (s, 3H, **NH**), 2.49 (t, 6H, N **CH_2**), 2.457 (t, 6H, NCH_2 **CH_2**), 3.88 (s, 6H, Ar **CH_2**). This data well consistent with the previously reported data[40].

Optimized synthesis of tripodal crosslinker. In the second step, an oven-dried scintillation vial equipped with a magnetic stir bar was charged with a suitable amount of β-CD (0.624 g, 0.55 mmol, 1 equiv), TriPod crosslinker (0.75 g, 1.1 mmol, 2 equiv), K_2CO_3 (1.520 g, 11 mmol, 20 equiv), and 3.6 mL anhydrous DMSO. The vial was placed on a preheated hot-stirring plate (85 °C) and stirred at 500 rpm for 24 h. Gelation was observed within 3 h. The vial was cooled, and the crude product was filtered, neutralized with HCl, and then washed by stirring in deionized H_2O (2 × 10 mL) for 10 min, THF (2 × 10 mL) for 10 min, and CH_2Cl_2 (1 × 10 mL) for 10 min. The filtered solid was packed into a teabag and activated by Soxhlet extraction with methanol for one day. The solid was dried in a vacuum oven to obtain the final product powder. The schematic presentation of β-CD-TriPod polymeric adsorbent is illustrated in Fig. 1.

Characterization of β-CD-TriPod adsorbent

The surface functional groups of the synthesized β−CD−TriPod polymer were examined using Fourier transform infrared spectroscopy (FT–IR),

Nexus 670, Thermo Electron Corporation, United States, in the range of 675–4000 cm^{-1}.

1H NMR spectra were measured on a Varian VNMRS (600 MHz) spectrometer (International Equipment Trading Ltd., USA) at 298 K using $CDCl_3$ as the solvent.

The surface morphology and structure information were examined using field-emission scanning electron microscopy (FESEM) (SU−8010, Hitachi, Japan) at a working voltage of 2.0 kV voltage. Thermo Scientific Ultra Dry SDD attached with FESEM was used to analyze elemental compositions using an energy dispersive X-ray spectrometer (EDS). Gold coating was carried out to make the surface conducting for both FESEM and elemental analysis.

TGA was performed on EXSTAR 6300, (Japan) with a heating rate of 10 °C min^{-1} from 40 °C to 700 °C under a nitrogen environment.

Qualitative determination of the TriPod cross-linker was performed using a mass spectrometer (LCMS-8050TM; Shimadzu, Kyoto, Japan) via flow injection without column separation.

Quantification of the used PFASs (10 ng L^{-1} to 200 ng L^{-1}) from the adsorption studies in aqueous solution was performed using ultra-high-performance liquid chromatography tandem mass spectrometry (LC-MS/MS) coupled with electrospray ionization (LCMS-8050™, Shimadzu, Kyoto, Japan). Details quantification process of the used PFASs are provided in Text SI-2.

Batch adsorption experiments

A series of batch adsorption experiments was conducted to optimize the adsorption efficiency and capacity for PFASs removal at 24 °C in a multi-position incubator (DAIHAN Scientific, South Korea) with a shaking rate of 200 revolutions per minute (rpm). Aqueous samples from adsorption experiments were filtered with a 0.20 µm cellulose acetate syringe filter for analysis. Detailed procedures and conditions for all the experiments are provided in Text SI-3.

The PFAS removal efficiency by the adsorbent was determined by Eq. 1:

$$\text{Removal}(\%) = \frac{(C_0 - C_t) \times 100}{C_0} \quad (1)$$

where C_0 (ng L^{-1}) and C_t (ng L^{-1}) are the initial and residual concentration of PFAS in the stock solution and filtrate, respectively.

The amount of PFAS bound to the sorbent was determined using Eq. 2:

$$\text{Adsorption capacity}\,(q_t) = \frac{(C_0 - C_t)}{C_A} \quad (2)$$

where q_t (mg g^{-1}) is the amount of PFAS adsorbed on the solid phase at any time t (h); C_0 (ng L^{-1}) is the initial concentration of the PFAS in the samples; C_t (ng L^{-1}) is the concentration of the PFAS in the liquid phase at any sample time t (h); and C_A (mg L^{-1}) is the concentration of adsorbent.

The batch kinetics of higher concentrations can be described using pseudo-first-order (PFO) and PSO models in a non-linearized form, proposed by Lagergren[42] and Ho and McKay[43] models, as shown in Eqs. 3 and 4, respectively.

$$q_t = q_e(1 - e^{-k1t}) \quad (3)$$

$$q_t = \frac{k_2 q_e^2 t}{1 + q_e k_2 t} \quad (4)$$

where q_t (mg g^{-1}) and q_e (mg g^{-1}) are the amount of PFAS adsorbed on the solid phase adsorbent at time t and at equilibrium, respectively. k_1 (h^{-1}) and k_2 (g mg^{-1} h^{-1}) are the PFO and PSO adsorption rate constants, respectively.

Two well-known isotherm models, Langmuir and the Freundlich adsorption isotherm fits, were generated using nonlinear least squares regression.

Langmuir. The Langmuir isotherm model is widely applicable to a homogeneous adsorption surface, where each adsorption site can only bind to one adsorbate. Langmuir model in the non-linear form is given in Eq. 5:

$$q_e = \frac{q_m K_L C_e}{1 + K_L C_e} \quad (5)$$

where q_e (mg g^{-1}) is the amount of PFAS adsorbed at equilibrium, q_m (mg g^{-1}) is the maximum adsorption capacity of the adsorbent at equilibrium, C_e (mg L^{-1}) is the residual PFAS concentration at equilibrium, and K_L (L mg^{-1}) is the Langmuir constant concerning adsorption energy.

Freundlich. Freundlich isotherm model assumes a heterogeneous surface and a non-uniform distribution of adsorption heat over the surface without saturation of the adsorption sites. The nonlinear form of the Freundlich model is represented by Eq. 6.

$$q_e = K_F C_e^{1/n} \quad (6)$$

where q_e (mg g^{-1}) is the amount of PFAS adsorbed at equilibrium, C_e (mg L^{-1}) is the residual PFAS concentration in the aqueous phase at equilibrium, K_F [(mg g^{-1}) (L mg^{-1})$^{1/n}$] is Freundlich constant, n indicates the adsorption intensity, and the magnitude of n reflects whether the uptake characteristics are good ($2 < n < 10$), difficult ($1 < n < 2$), or poor ($n < 1$).

β−CD-TriPod regeneration experiments

Fifty milligrams β−CD-TriPod was added to an Erlenmeyer flask containing a PFOS solution (100 mL, 200 µg L^{-1}). The adsorption experiments were conducted at 24 °C in an incubator for 6 h at a stirring rate of 200 rpm. The resulting suspension was filtered through Whatman filter paper, and the residual PFAS concentrations were measured by LC-MS. Afterwards, PFASs-loaded β−CD-TriPod was regenerated by soaking in 50 mL MeOH for 24 h and recovered by filtration. The MeOH filtrate was concentrated under vacuum, and the residual solid was dissolved in 100 mL of deionized H_2O and analyzed by LC-MS to determine the amount of recovered PFOS.

Data availability

All data used in this study are available in this paper and in the supplementary information.

Received: 27 June 2025; Accepted: 1 September 2025;
Published online: 13 October 2025

References

1. Wang, R. et al. A tunable porous β-cyclodextrin polymer platform to understand and improve anionic PFAS removal. *ACS Cent. Sci.* **8**, 663–669 (2022).
2. Evich, M. G. et al. Per- and polyfluoroalkyl substances in the environment. *Science***375**, 1–14 (2022).
3. Song, C. et al. Multifunctionalized covalent organic frameworks for broad-spectrum extraction and ultrasensitive analysis of per- and polyfluoroalkyl substances. *Anal. Chem.* **95**, 7770–7778 (2023).
4. Ching, C., Klemes, M. J., Trang, B., Dichtel, W. R. & Helbling, D. E. β-cyclodextrin polymers with different cross-linkers and ion-exchange resins exhibit variable adsorption of anionic, zwitterionic, and nonionic PFASs. *Environ. Sci. Technol.* **54**, 12693–12702 (2020).
5. Leung, S. C. E., Wanninayake, D., Chen, D., Nguyen, N. T. & Li, Q. Physicochemical properties and interactions of perfluoroalkyl substances (PFAS)—challenges and opportunities in sensing and remediation. *Sci. Total Environ.* **905**, 166764 (2023).
6. Nakayama, S. F. et al. Worldwide trends in tracing poly- and perfluoroalkyl substances (PFAS) in the environment. *TrAC Trends Anal. Chem.* **121**, 115410 (2019).

7. Wang, Z., Cousins, I. T., Scheringer, M. & Hungerbuehler, K. Hazard assessment of fluorinated alternatives to long-chain perfluoroalkyl acids (PFAAs) and their precursors: status quo, ongoing challenges and possible solutions. *Environ. Int.* **75**, 172–179 (2015).
8. Ateia, M., Maroli, A., Tharayil, N. & Karanfil, T. The overlooked short- and ultrashort-chain poly- and perfluorinated substances: a review. *Chemosphere* **220**, 866–882 (2019).
9. Verma, M. et al. Chitosan cross-linked β–cyclodextrin polymeric adsorbent for the removal of perfluorobutanesulfonate from aqueous solution: adsorption kinetics, isotherm, and mechanism. *Environ. Sci. Pollut. Res.* **30**, 19259–19268 (2023).
10. Cantoni, B., Turolla, A., Wellmitz, J., Ruhl, A. S. & Antonelli, M. Perfluoroalkyl substances (PFAS) adsorption in drinking water by granular activated carbon: influence of activated carbon and PFAS characteristics. *Sci. Total Environ.* **795**, 148821 (2021).
11. McCleaf, P. et al. Removal efficiency of multiple poly- and perfluoroalkyl substances (PFASs) in drinking water using granular activated carbon (GAC) and anion exchange (AE) column tests. *Water Res.* **120**, 77–87 (2017).
12. Rizzo, L. et al. Consolidated vs new advanced treatment methods for the removal of contaminants of emerging concern from urban wastewater. *Sci. Total Environ.* **655**, 986–1008 (2019).
13. Zhang, D. Q., Zhang, W. L. & Liang, Y. N. Adsorption of perfluoroalkyl and polyfluoroalkyl substances (PFASs) from aqueous solution—a review. *Sci. Total Environ.* **694**, 133606 (2019).
14. Kennedy, A. M., Reinert, A. M., Knappe, D. R. U., Ferrer, I. & Summers, R. S. Full- and pilot-scale GAC adsorption of organic micropollutants. *Water Res.* **68**, 238–248 (2015).
15. Zaggia, A., Conte, L., Falletti, L., Fant, M. & Chiorboli, A. Use of strong anion exchange resins for the removal of perfluoroalkylated substances from contaminated drinking water in batch and continuous pilot plants. *Water Res.* **91**, 137–146 (2016).
16. Shahrokhi, R. & Park, J. Enhanced removal of short- and long-chain per- and poly-fluoroalkyl substances from aqueous phase using crushed grafted chitosan beads: performance and mechanisms. *Environ. Pollut.* **340**, 122836 (2024).
17. Wang, W. et al. Rapid removal of perfluoroalkanesulfonates from water by β-cyclodextrin covalent organic frameworks. *ACS Appl. Mater. Interfaces* **13**, 48700–48708 (2021).
18. Liu, Q., Zhou, Y., Lu, J. & Zhou, Y. Novel cyclodextrin-based adsorbents for removing pollutants from wastewater: a critical review. *Chemosphere* **241**, 125043 (2020).
19. Xiao, L. et al. -Cyclodextrin polymer network sequesters perfluorooctanoic acid at environmentally relevant concentrations. *J. Am. Chem. Soc.* **139**, 7689–7692 (2017).
20. Li, R. et al. Efficient removal of per- and polyfluoroalkyl substances from water with zirconium-based metal-organic frameworks. *Chem. Mater.* **33**, 3276–3285 (2021).
21. Zhang, Y. et al. A porphyrinic metal-organic framework with cooperative adsorption domains for PFAS removal from water. *ChemSusChem* **17**, e202400069 (2024).
22. Huang, J. et al. Facile synthesis of a fluorinated-squaramide covalent organic framework for the highly efficient and broad-spectrum removal of per- and polyfluoroalkyl pollutants. *Angew. Chem. Int. Ed.* **61**, 1–5 (2022).
23. Crini, G. Review: a history of cyclodextrins. *Chem. Rev.* **114**, 10940–10975 (2014).
24. Klemes, M. J. et al. Polymerized molecular receptors as adsorbents to remove micropollutants from water. *Acc. Chem. Res.* **53**, 2314–2324 (2020).
25. Alsbaiee, A. et al. Rapid removal of organic micropollutants from water by a porous β-cyclodextrin polymer. *Nature* **529**, 190–194 (2016).
26. Choudhary, A., Dong, D., Tsianou, M., Alexandridis, P. & Bedrov, D. Adsorption mechanism of perfluorooctanoate on cyclodextrin-based polymers: probing the synergy of electrostatic and hydrophobic interactions with molecular dynamics simulations. *ACS Mater. Lett.* **4**, 853–859 (2022).
27. Klemes, M. J. et al. Reduction of a tetrafluoroterephthalonitrile-β-cyclodextrin polymer to remove anionic micropollutants and perfluorinated alkyl substances from water. *Angew. Chem. Int. Ed.* **58**, 12049–12053 (2019).
28. Weiss-Errico, M. J. & O'Shea, K. E. Detailed NMR investigation of cyclodextrin-perfluorinated surfactant interactions in aqueous media. *J. Hazard. Mater.* **329**, 57–65 (2017).
29. Klemes, M. J. et al. Phenolation of cyclodextrin polymers controls their lead and organic micropollutant adsorption. *Chem. Sci.* **9**, 8883–8889 (2018).
30. Li, J. et al. Efficient adsorption of BPA and Pb2+ by sulfhydryl-rich β-cyclodextrin polymers. *Sep. Purif. Technol.* **309**, 122913 (2023).
31. Yu, Q., Zhang, R., Deng, S., Huang, J. & Yu, G. Sorption of perfluorooctane sulfonate and perfluorooctanoate on activated carbons and resin: kinetic and isotherm study. *Water Res.* **43**, 1150–1158 (2009).
32. Zhang, D. et al. Sorption of perfluorooctanoic acid, perfluorooctane sulfonate and perfluoroheptanoic acid on granular activated carbon. *Chemosphere* **144**, 2336–2342 (2016).
33. Ateia, M., Alsbaiee, A., Karanfil, T. & Dichtel, W. Efficient PFAS removal by amine-functionalized sorbents: critical review of the current literature. *Environ. Sci. Technol. Lett.* **6**, 688–695 (2019).
34. Ji, W. et al. Removal of GenX and perfluorinated alkyl substances from water by amine-functionalized covalent organic frameworks. *J. Am. Chem. Soc.* **140**, 12677–12681 (2018).
35. Wu, C., Klemes, M. J., Trang, B., Dichtel, W. R. & Helbling, D. E. Exploring the factors that influence the adsorption of anionic PFAS on conventional and emerging adsorbents in aquatic matrices. *Water Res.* **182**, 115950 (2020).
36. Wang, W. et al. Adsorption behaviour and mechanism of the PFOS substitute OBS (sodium p-perfluorous nonenoxybenzene sulfonate) on activated carbon. *R. Soc. Open Sci.* **6**, 191069 (2019).
37. Verma, M. et al. β-Cyclodextrin polymerization for selective separation of long chain per- and poly fluorinated alkyl substances at environmentally level concentrations. *Sep. Purif. Technol.* **379**, 134917. https://doi.org/10.1016/j.seppur.2017.11.073.
38. Kunsan Air Base. *Drinking Water Quality Annual Report for Calendar Year 2022*, *Gwangju Air Base* 1–7 (2023).
39. Deng, S. et al. Enhanced adsorption of perfluorooctane sulfonate and perfluorooctanoate by bamboo-derived granular activated carbon. *J. Hazard. Mater.* **282**, 150–157 (2015).
40. Lakshminarayanan, P. S., Ravikumar, I., Suresh, E. & Ghosh, P. Encapsulation of halides within the cavity of a pentafluorophenyl-substituted tripodal amine receptor. *Inorg. Chem.* **46**, 4769–4771 (2007).
41. Yang, A., Ching, C., Easler, M., Helbling, D. E. & Dichtel, W. R. Cyclodextrin polymers with nitrogen-containing tripodal crosslinkers for efficient PFAS adsorption. *ACS Mater. Lett.* **2**, 1240–1245 (2020).
42. Lagergren, S. About the theory of so-called adsorption of soluble substances. *Proc. R. Swed. Acad. Sci.* **24**, 1–39 (1898).
43. Ho, Y. S. & McKay, G. Pseudo-second order model for sorption processes. *Process Biochem.* **34**, 451–465 (1999).

Acknowledgements

Monu Verma thanks the National Research Foundation of Korea (NRF) for the funding provided by the Ministry of Science and ICT through the Brain Pool Program (RS-2024-00406513). H. Kim was supported by the Korea Ministry of Environment (MOE) for providing financial support by the grant under developing innovative drinking water and wastewater technologies (2019002710006) and the Graduate Program specialized in Post-plastics Era, and was also supported by the 2022 sabbatical year research grant of

the University of Seoul. This paper has been supported by the RUDN University Strategic Academic Leadership Program.

Author contributions

M. Verma: conceptualization, experimental design, and writing the original draft. Y. Hong: analysis and editing. K.P. Singh, S.Y. Pan, C. Li, G.K. Rao, M. Nanda, and S.K. Arora: editing and review. V. Kumar: investigation and review, and H. Kim: supervising, review and editing.

Competing interests

The authors declare no competing interests.

Additional information

Supplementary information The online version contains supplementary material available at https://doi.org/10.1038/s41545-025-00519-6.

Correspondence and requests for materials should be addressed to Hyunook Kim.